Traveling-wave tubes and backward-wave oscillators with weak external magnetic fields

T. M. Abu-elfadl, G. S. Nusinovich, A. G. Shkvarunets, Y. Carmel, and T. M. Antonsen, Jr.
Institute for Plasma Research, University of Maryland at College Park, College Park, Maryland 20742-3511

D. Goebel
Boeing EDD Inc., 3100 West Lomita Boulevard, Torrance, California 90505
(Received 20 December 2000; published 23 May 2001)

Recent development of plasma-assisted slow-wave oscillators [Goebel *et al.* IEEE Trans. Plasma Sci. **22**, 547 (1994)], microwave sources that operate without guiding magnetic fields, has stimulated interest in the theoretical analysis of such tubes. In principle, in the absence of guiding magnetic fields, due to the space charge forces and the radial electric field of the wave, the electrons may propagate radially outward which increases electron coupling to the slow wave whose field is localized near the slow-wave structure (SWS). This increases the wave growth rate and efficiency, and hence allows one to shorten the interaction region. So the radial electron motion can be beneficial for operation if it does not lead to interception of electrons by the SWS. To avoid this interception a weak external magnetic field can be applied. The theory developed describes the effect of weak magnetic fields on the operation of traveling-wave tubes and backward-wave oscillators with electrons moving not only axially but also transversely. This theory allows one to estimate the magnetic field required for protecting the SWS from electron bombardment at different power levels. Theoretical predictions of the efficiency enhancement due to the weak magnetic field are confirmed in experiments.

DOI: 10.1103/PhysRevE.63.066501 PACS number(s): 41.60.Bq, 84.40.Fe, 52.59.Ye, 07.57.Hm

I. INTRODUCTION

Both traveling-wave tubes and backward-wave oscillators can be considered as sources of coherent Cherenkov radiation. The operation of these devices is based on the synchronous interaction between an electron beam and an em wave. A slow-wave structure is employed to reduce the phase velocity of the em wave, v_{ph}, to the axial velocity of the electrons, v_z, thus providing the condition for Cherenkov interaction. In most of these devices a strong axial magnetic field is applied to guide the electron beam. Correspondingly, only one-dimensional interaction is allowed between the axially streaming electrons and the axial electric field of the wave. Applying such a strong magnetic field requires heavy and bulky solenoids. Recently, devices called PASOTRON's (plasma-assisted slow-wave oscillators) [1,2] have been developed. These devices usually operate without a guiding magnetic field. The beam transport is provided by the presence of ions which compensate for the space charge forces and thus cause the ion focusing known as the Bennett pinch [3].

Even in the case of complete compensation of electron space charge fields, the absence of a strong external magnetic field allows electrons to move radially under the action of the radial electric field of the wave. This can cause two effects: (a) radial motion outward increases the coupling impedance, and (b) transverse interaction increases the growth rate. The linear theory of this interaction was considered in [4]. In the large-signal regime, however, this transverse degree of freedom may cause electron interception by the slow-wave structure (SWS). It was shown both in theory [5] and experiments [1,2] that at large wave intensities a significant part of the electrons can be intercepted by the SWS, which may damage it. It seems possible to avoid this interception and, at the same time, to benefit from electron transverse motion by using a weak external magnetic field. The theoretical and experimental study of this possibility is the purpose of the present paper.

In our theoretical study we follow the model presented in [5] with the addition of a weak magnetic field. We will show that this magnetic field provides some kind of tuning to the device, where higher power without electron interception can be achieved. This tuning can be done by varying the magnetic field strength simultaneously with other parameters of the device in an attempt to attain higher power over an interception-free length. Providing some tapering could even enhance the device operation more by achieving the maximum power over a shorter length. It will be shown that a weak axial magnetic field can enhance the efficiency of both traveling-wave tubes (TWT's and backward-wave oscillators BWO's).

The paper is organized as follows. In Sec. II, the formulation of the problem is presented, where the equations describing the electron dynamic and wave evolution are derived. A simplified model is also presented. The dispersion relation for a TWT in the presence of a uniform axial magnetic field is presented in Sec. III. The results of the nonlinear theory for TWT's and BWO's are presented in Sec. IV, where Secs. IV A and IV B are for TWT's and BWO's, respectively. In Sec. V we present experimental data describing the operation of the PASOTRON-BWO with a weak magnetic field. The conclusion is presented in Sec. VI.

II. FORMULATION

For symmetric periodic structures, the nonzero components of the symmetric transverse magnetic mode TM_{0p} in accordance with the Flouqet theorem are

$$E_z = \mathrm{Re}\left\{ e^{-i\omega t} \sum_n -a_n \frac{g_n}{\omega/c} I_0(g_n r) e^{ik_{zn}z} \right\}, \qquad (1)$$

$$E_r = \mathrm{Re}\left\{ e^{-i\omega t} \sum_n \; i a_n \frac{k_{zn}}{\omega/c} I_1(g_n r) e^{i k_{zn} z} \right\},$$

$$B_\phi = \mathrm{Re}\left\{ e^{-i\omega t} \sum_n \; i a_n I_1(g_n r) e^{i k_{zn} z} \right\}.$$

Here $k_{zn} = k_{z0} + 2\pi n/d$ is the axial wave number of the nth space harmonic (d is the structure period), and $g_n = \sqrt{k_{zn}^2 - (\omega/c)^2}$ is the transverse wave number of a slow wave.

The equations of motion for a charge q moving in the electromagnetic field of a TM mode and a dc axial magnetic field $B_0 \mathbf{e_z}$ can be written in cylindrical coordinates as

$$\frac{dp_r}{dt} - \gamma m r \dot{\phi}^2 = q\left(E_r + \frac{r\dot{\phi}}{c} B_0 - \frac{p_z}{\gamma m c} B_\phi \right), \tag{2a}$$

$$\frac{1}{r}\frac{d}{dt}(\gamma m r^2 \dot{\phi}) = -\frac{q}{c} \dot{r} B_0, \tag{2b}$$

$$\frac{dp_z}{dt} = q\left(E_z + \frac{p_r}{\gamma m c} B_\phi \right), \tag{2c}$$

$$\gamma = \sqrt{1 + \frac{1}{m^2 c^2}(p_r^2 + \gamma^2 m^2 r^2 \dot{\phi}^2 + p_z^2)}. \tag{2d}$$

From Eq. (2b), we can get a constant of motion (the azimuthal canonical momentum P_ϕ), which is

$$P_\phi = \gamma m r^2 \dot{\phi} + \frac{q}{c}\frac{r^2}{2} B_z(z) = \text{const.}$$

If we assume that at the entrance the electron beam is annular and thin with an initial radius r_0, and all initial electron velocities are axial ($\dot{\phi}_0 = 0$), then the constant of motion is $q r_0^2 B_0 / 2c$. So the equation for $\dot{\phi}$ becomes

$$\dot{\phi} = \frac{qB_0}{2\gamma m r^2 c}(r_0^2 - r^2).$$

With this equation we can eliminate $\dot{\phi}$ from Eqs. (2). We will also take the independent variable z instead of t, and introduce the slowly variable phase $\theta = k_{z,synch} z - \omega t$, where $k_{z,synch}$ is the axial wave number corresponding to the synchronous space harmonic of the wave field in the expansion Eqs. (1). For simplicity we normalize the coordinates z and r by ω/c, and the momenta p_z and p_r by $1/mc$. Also, in the equations of motion (2), we keep only the synchronous harmonic in the field expansion (1), since we assume that the rest of the harmonics are asynchronous with the electron beam. So Eqs. (2) become

$$\frac{dp_r}{dz} = \Omega^2 \frac{r_0^4 - r^4}{p_z r^3} + \left(h\frac{\gamma}{p_z} - 1 \right) \hat{I}_1(\kappa r) \mathrm{Im}\{A e^{i\theta}\}, \tag{3a}$$

$$\frac{dp_z}{dz} = \frac{\gamma}{p_z} \kappa \hat{I}_0(\kappa r) \mathrm{Re}\{A e^{i\theta}\} + \frac{p_r}{p_z} \hat{I}_1(\kappa r) \mathrm{Im}\{A e^{i\theta}\}, \tag{3b}$$

$$\frac{dr}{dz} = \frac{p_r}{p_z}, \quad \frac{d\theta}{dz} = \Delta + \frac{\gamma_0}{p_{z0}} - \frac{\gamma}{p_z}, \tag{3c}$$

$$\gamma = \sqrt{1 + p_r^2 + \Omega^2 [r_0^2 - r^2 f(z)]^2 / r^2 + p_z^2}. \tag{3d}$$

We have added the two Eqs. (3c) to complete the system of equations. In these equations Δ is the detuning factor $\Delta = 1/\beta_{ph} - 1/\beta_{z0}$, where β_{ph} and β_{z0} are, respectively, the wave phase velocity of the synchronous harmonic and the initial electron axial velocity normalized to the speed of light. In Eqs. (3), we introduced the normalized nonrelativistic Larmor frequency $\Omega = \omega_L/\omega = eB_0/(2cm\omega)$, and the normalized field amplitude $A = eaI_0(gr_0)/(m\omega c)$, where g is the transverse wave number corresponding to the synchronous harmonic $k_{z,synch}$ ($g = \sqrt{k_{z,synch}^2 - \omega^2/c^2}$). Here the modified Bessel function $I_0(gr_0)$ describes the coupling of the axial electric field of the wave to electrons initially located at r_0, which corresponds to consideration of an initially thin annular electron beam. Also, we normalized the modified Bessel functions to $I_0(gr_0)$: $\hat{I}_0(gr) = I_0(gr)/I_0(gr_0)$, $\hat{I}_1(gr) = I_1(gr)/I_0(gr_o)$. In Eqs. (3a) and (3b) $h = k_{z,synch}/(\omega/c)$ and $\kappa = g/(\omega/c)$.

As is known, the equation describing the wave excitation can be obtained from the Maxwell equations. In the stationary regime, after some manipulations and considering only the synchronous harmonic, this yields the equation for the time independent wave amplitude, which for the TWT has the form [5]

$$\frac{\partial A}{\partial z} = -I \frac{1}{2\pi} \int_{2\pi} \left[\kappa \hat{I}_0(\kappa r) + i \frac{p_r}{p_z} h \hat{I}_1(\kappa r) \right] e^{-i\theta} d\theta_0. \tag{4}$$

In Eq. (4), we introduced $I = e2I_b I_0^2(gr_{b0})/(m\omega^2 N)$, where the norm of the wave N is proportional to the power of the propagating wave. The second term inside the square brackets represents the transverse interaction between the radial electron motion and the radial electric field of the em wave. For the BWO the minus sign in the right-hand side of Eq. (4) should be replaced by plus because in the BWO the wave propagates in the opposite direction.

In principle, Eqs. (3) and (4) form a self-consistent set of equations which can be integrated numerically. However, for the sake of simplicity, we can impose further assumptions. Let us assume $p_\perp \ll p_z$, where $p_\perp$ is the transverse momentum. By using this assumption Eqs. (3) and (4) can be reduced to

$$\frac{d^2\theta}{d\zeta^2} = \hat{I}_0(\rho) \mathrm{Re}\{\alpha e^{i\theta}\}, \tag{5a}$$

$$\frac{d^2\rho}{d\zeta^2} = \hat{I}_1(\rho) \mathrm{Im}\{\alpha e^{i\theta}\} + M \frac{\rho_0^4 - \rho^4}{\rho^3}, \tag{5b}$$

$$\frac{\partial \alpha}{\partial \zeta} = -\frac{1}{2\pi}\int_{2\pi} \hat{I}_0(\rho) e^{-i\theta}\, d\theta_0. \tag{5c}$$

In Eqs. (5) we introduced the Pierce-like gain parameter C, given by $C^3 = I/(\gamma_0^2 - 1)^{5/2}$, and used the normalization $\zeta = Cz$, $\rho = \kappa r$, and $\alpha = A/[C^2(\gamma_0^2 - 1)^2]$. We also introduced the magnetic field parameter $M = \Omega^2/(C^2\gamma_0^2\beta_0^2)$ (for $M = 0$ this set of equations reduces to those given in [5]).

Equations (3) and (4) can be used to calculate the efficiency

$$\eta = (\gamma_0 - \langle\gamma\rangle)/(\gamma_0 - 1).$$

Here, the angular brackets indicate averaging over the electron phases θ at the entrance. These equations also allow one to derive the energy conservation law that describes the correspondence between the changes in the beam energy given by the efficiency η and the changes in the wave intensity $|A|^2$. For the TWT this relation is given by

$$|A|^2 - |A_0|^2 = 2I(\gamma_0 - 1)\eta. \tag{6}$$

For the BWO with well matched ends, a similar relation is given by

$$|A_0|^2 = 2I(\gamma_0 - 1)\eta. \tag{7}$$

Here $|A_0|^2$ is the wave intensity at the entrance, while at the well matched exit the backward-wave intensity equals zero. Note that, when we use the simplified Eqs. (5) instead of Eqs. (3) and (4), the efficiency η can be given as

$$\eta = (\gamma_0 + 1)\sqrt{\gamma_0^2 - 1}\, C\, \hat{\eta}, \tag{8}$$

where $\hat{\eta} = \Delta - \langle d\theta/d\zeta\rangle$. Correspondingly, Eqs. (6) and (7) can be reduced to $\hat{\eta} = (|\alpha|^2 - |\alpha_0|^2)/2$ for the TWT case and $\hat{\eta} = |\alpha_0|^2/2$ for the BWO case. These relations are the same whether we have a guiding dc magnetic field or not [5].

Finally, let us show the relation between our Pierce-like gain constant C and the well known Pierce gain C_p given by

$$C_p^3 = \frac{I_b Z_c}{4V_b}.$$

Here I_b is the beam current, Z_c is the interaction impedance between the electron beam and electromagnetic slow wave, and V_b is the beam voltage. The relation between C and C_b can be shown to be

$$C^3 = \frac{4\gamma_0^2(\gamma_0 - 1)}{(\gamma_0^2 - 1)^{5/2}} C_p^3.$$

III. SMALL-SIGNAL ANALYSIS

By linearizing Eqs. (3) and (4), one can derive the dispersion equation describing the propagation of em perturbations through the system. We assume the perturbations in em wave and electron motion to have axial dependence $\exp(i\Gamma z)$. After some mathematical manipulations, this yields the following dispersion equation:

$$\left[(\Gamma - \Delta)\Gamma^2 + \frac{C^3}{2}\right]\left(\Gamma^2 - \frac{4\Omega^2}{\gamma_0^2\beta_{z0}^2}\right) - \frac{C^3}{2}q^2\Gamma^2(\Gamma\beta_{z0}\gamma_0^2 - 1) = 0, \tag{9}$$

where $q = I_1^2(|g|r_{b0})/I_0^2(|g|r_{b0})$. In the case of zero magnetic field ($\Omega = 0$), Eq. (9) reduces to that derived in [5].

For small C's, we can introduce $\gamma = 2^{1/3}\Gamma/C$, $\delta = 2^{1/3}\Delta/C$, $\Omega_B = 2^{1/3}(2\Omega)/(\gamma_0\beta_{z0}C)$. Then ignoring the small term $\Gamma\beta_{z0}\gamma_0^2 \sim C\gamma$ reduces Eq. (9) to

$$[(\gamma - \delta)\gamma^2 + 1](\gamma^2 - \Omega_B^2) + q^2\gamma^2 = 0. \tag{10}$$

Note that, since this equation was extensively studied in Ref. [4], there is no reason to repeat this study in our paper. Equation (10) is essentially the same as Eq. (13.26) in [4]: our parameters γ, δ, Ω_0^2, and q^2 correspond to Pierce parameters $i\delta$, b, f^2, and α^2, respectively.

Recall that the study done in [4] showed that, as the magnetic field increases, the wave growth rate becomes smaller and it has a maximum at larger detuning δ. For instance, when $\Omega_0^2 = 0$ $(\mathrm{Im}\,\gamma)_{\max} = \sqrt{3}/2$ and $\delta_{\mathrm{opt}} = 0$, while when $\Omega_0^2 = 10$ $(\mathrm{Im}\,\gamma)_{\max} \simeq 0.39$ and $\delta_{\mathrm{opt}} \simeq 3.2$. Also note that in Eq. (9), which can be rewritten, in accordance with [4], as

$$\gamma - \delta = -\frac{1}{\gamma^2} - \frac{q^2}{\gamma^2 - \Omega_B^2}, \tag{11}$$

we ignored space charge effects. This assumption is quite reasonable for moderate magnetic fields, which are the focus of our present study. However, at large magnetic fields the last term in Eq. (11) decreases, and correspondingly the validity of the neglect of space charge effects should be accurately analyzed.

IV. NONLINEAR RESULTS

A. Traveling-wave tube

Equations (5) can be integrated to obtain the wave amplitude evolution with axial distance. Figures 1 show the evolution of $|\alpha|$ versus ζ for different values of the magnetic field parameter M. In Figs. 1 the device parameters are electron beam initial radius $\rho_0 = 2.0$, wave initial amplitude $\alpha_0 = 0.03$, and SWS radius $\rho_{\mathrm{SWS}} = 4.0$. The saturation of the growth of $|\alpha|$ is mainly due to electron interception by the SWS. The interception starts near the maximum of $|\alpha|$. We are interested in achieving the maximum before electron interception by the SWS, because electron interception by the SWS may cause rf breakdown. So adding an axial magnetic field can increase the traveling distance of electrons before hitting the SWS, and hence increase the maximum wave amplitude that can be achieved before interception.

Further illustration of the effect of the magnetic field is shown in Figs. 2 and 3 for different initial values of $|\alpha|$, where the contours of $|\alpha_{\max}|$ are shown in the plane of the magnetic field parameter M versus the normalized detuning

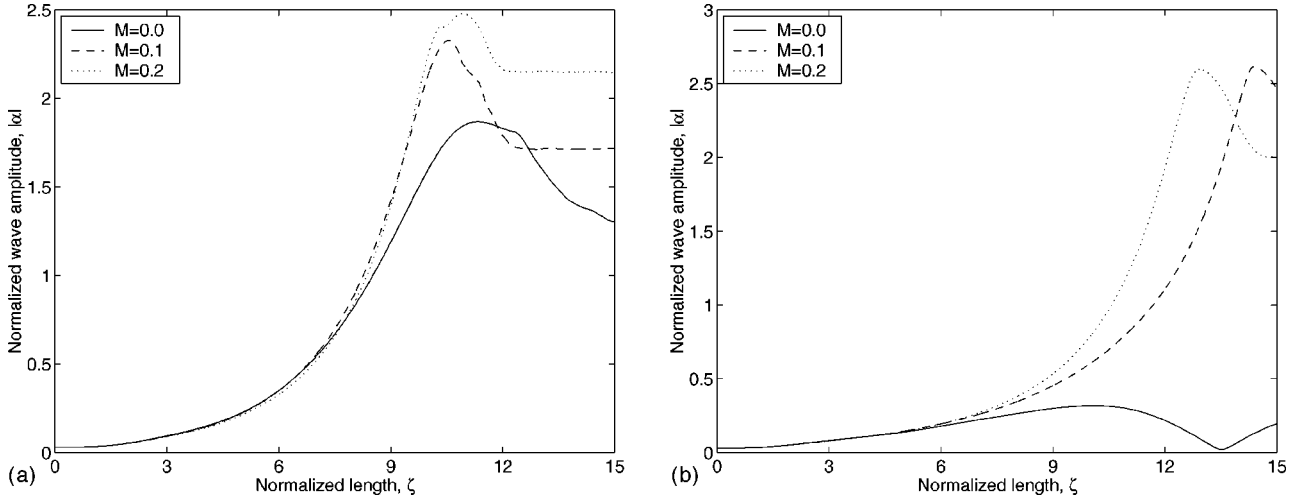

FIG. 1. The normalized wave amplitude profile for a TWT for various values of the magnetic field parameter M. The parameters of the device $\rho_0=2.0$, $\alpha_0=0.03$. (a) for detuning $\Delta=1.5$, and (b) for detuning $\Delta=1.7$.

Δ. All the simulation results are obtained for $r_{SWS}=2r_0$, where r_{SWS} and r_0 are the SWS interception radius (the radial distance to the SWS) and the electron initial radius, respectively. The corresponding normalized parameters are $\rho_0=2$ and $\rho_{SWS}=4$. It is clear from Figs. 2 and 3 that for fixed values of Δ, as we increase M, $|\alpha_{max}|$ initially increases until it reaches its peak. Then, if we further increase M, $|\alpha_{max}|$ decreases. This can be explained in the following way. The initial increase of M keeps the electrons from hitting the SWS for a longer length. So the em power is enhanced for an initial increase of M. Further increase in the magnetic field causes the electrons to be guided away from the SWS. This results in a reduction in the interaction impedance and, correspondingly, the maximum power. Note that, as follows from Figs. 2 and 3, even a rather weak magnetic field, which corresponds to $M\leqslant 0.1$, allows one to increase the maximum wave amplitude from less than 2.0 (for $M=0$) to 2.6. Since the efficiency, as shown above, is proportional to $|\alpha|^2$, this indicates an efficiency increase by a factor of 1.7 due to the presence of a weak magnetic field. (The estimates for the magnetic field for the BWO case will be given in Sec. IV B.) In the case of an infinitely strong magnetic field, as follows from [6], the maximum amplitude is equal to 2.52, which yields an efficiency that is 1.6 times larger than in the absence of B_0, but a little smaller than at $M\leqslant 0.1$.

It is always preferable to avoid interception until the maximum power is achieved, because electron interception by the SWS may cause rf breakdown, which leads to pulse shortening. We denote the distance where the first interception occurs by Z_{int} and the length corresponding to the maximum power ($|\alpha_{max}|$) by Z_{max}. In Figs. 2 and 3 the regions in the M-Δ plane where $Z_{int}>Z_{max}$ and $Z_{int}<Z_{max}$ are shown.

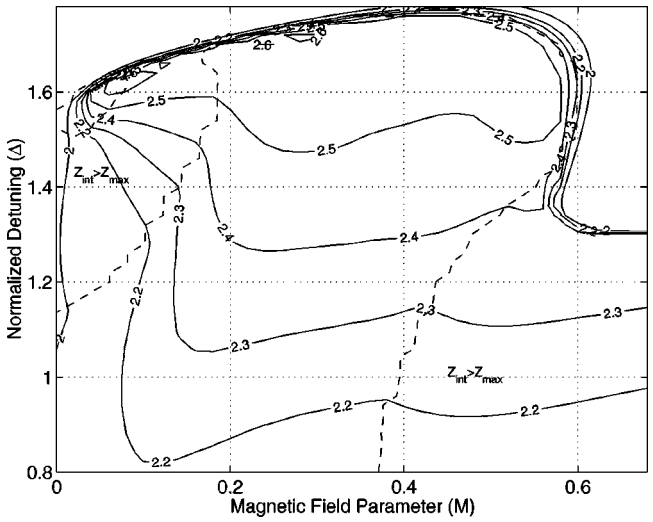

FIG. 2. TWT contours of $|\alpha_{max}|$. The initial conditions are $\rho_0=2.0$, $\alpha_0=0.003$, and the device normalized length is 20.0. The dashed lines indicate the border between the regions where the maximum amplitude can be reached without interception ($Z_{max}<Z_{int}$), and that where interception starts before reaching the maximum ($Z_{max}>Z_{int}$).

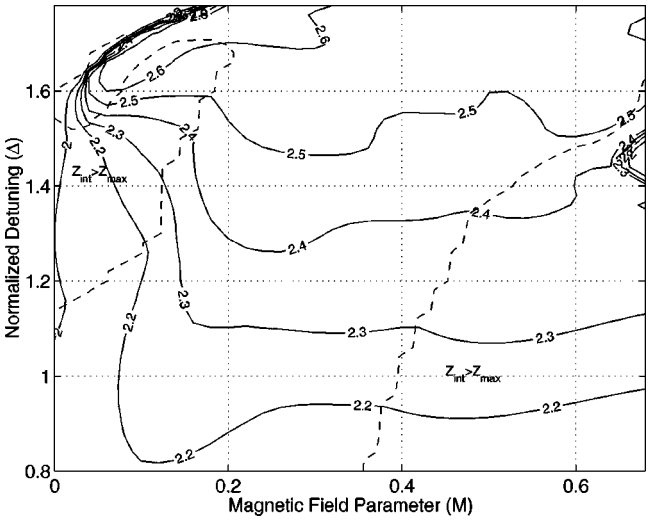

FIG. 3. TWT contours of $|\alpha_{max}|$. The initial conditions are $\rho_0=2.0$, $\alpha_0=0.03$, and the device normalized length is 15.0.

For interception-free operation of the device, the length of the device should be designed to be Z_{max}. So, to avoid rf breakdown due to interception, we should tune the device to operate in the region $Z_{int} > Z_{max}$. Note that, as shown in Figs. 2 and 3, at very different levels of the input power, when $\rho_0 = \rho_{SWS}/2$, it is possible to reach the maximum power ($|\alpha_{max}|$) without interception. In all the calculated results, we took $\rho_{SWS} = 4.0$. Our calculations also showed that, when the beam is initially located closer to the SWS (for instance, $\rho_0 = 3\rho_{SWS}/4$), the interception occurs earlier and restricts the amplitude growth.

If we have a tapered magnetic field $B_z = B_0 f(z)$, where $f(z)$ is the tapering function of the magnetic field [$f(z) = 1$ for uniform field], then Eq. (5b) becomes

$$\frac{d^2\rho}{d\zeta^2} = \hat{I}_1(\rho)\mathrm{Im}\{\alpha e^{i\theta}\} + M\frac{\rho_0^4 - \rho^4 f(\zeta)^2}{\rho^3}.$$

[Note that we ignored the radial magnetic field that appears in the region of axially inhomogeneous $B_z(z)$: $B_r = -dB_z/dz \times r/2$. Therefore the formulation is valid only for $df(\zeta)/d\zeta \ll 1$.] We assume that the tapering of the field is parabolic and it begins after length L_t. So $f(z)$ has the form

$$f(z) = \begin{cases} 1, & 0 < z < L_t \\ 1 + \left(\dfrac{z - L_t}{L - L_t}\right)^2 (s-1) & L_t < z < L. \end{cases}$$

Here L is the total interaction length of the device, $s = B_{min}/B_0$, and B_{min} is the minimum axial field, which occurs at $z = L$.

When the effect of tapering the magnetic field was studied, it showed that when tapering starts at the entrance (or near it) this reduces the optimum length of the device. This can be explained by considering the first region of electron transport as the bunching region, where electron bunches are formed due to interaction with the rf wave. For that region, to keep the electrons from hitting the SWS, a relatively large magnetic field is applied. In the second region the magnetic field is tapered and so these electron bunches can move radially toward the SWS, where the rf field is large. Therefore, radiation of these bunches increases as they approach the SWS.

B. Backward-wave oscillator

The equations for the BWO are the same as Eqs. (5), except for replacing Eq. (5c) for the evolution of α by

$$\frac{\partial\alpha}{\partial\zeta} = \frac{1}{2\pi}\int_{2\pi} \hat{I}_0(\rho) e^{-i\theta}\, d\theta_0.$$

To determine the axial profile of a backward-wave envelope, we solved these equations for different initial values of α_0 and for different normalized detunings Δ. We pick only the values of α_0 and Δ that result in a decrease of $|\alpha|$ to zero, as shown in Fig. 4. The normalized distance at which $|\alpha| = 0$ is denoted in Fig. 4 by ζ_0. If we choose our BWO with normalized length ζ_0 and assume its output to be matched, then

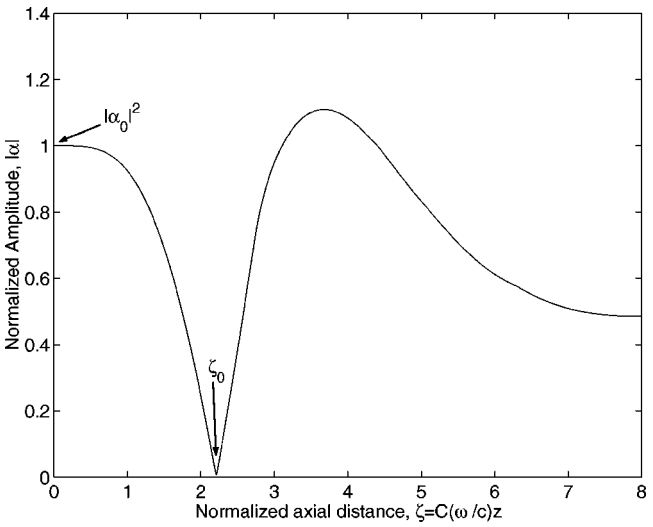

FIG. 4. Sample output of the evolution of $|\alpha|$ with ζ for a BWO. The parameters used are initial normalized beam radius $\rho_0 = 2.0$, detuning factor $\Delta = 1.48$, and normalized interception radius $\rho_{SWS} = 4.0$.

the solution with that specific α_0 and Δ corresponds to a possible operating mode. Figure 5 shows the value of $|\alpha|^2$ versus the normalized length ζ_0, for different values of the magnetic parameter M. For each value of M, there is a minimum length $\zeta_{0,min}$ below which there is no oscillation of the BWO. This length is known as the starting length of the BWO [7]. As seen in Fig. 5, this $\zeta_{0,min}$ slightly increases as we increase the magnetic field parameter M. The increase in $\zeta_{0,min}$ is due to the reduction in the coupling between the electrons and the rf wave with increase in the magnetic field parameter $M \propto B_0^2$.

In the absence of the axial magnetic field ($M = 0$) Fig. 5 shows that for large $|\alpha_0|^2$ (roughly for $|\alpha_0|^2 > 1.8$) there is interception of electrons by the SWS. The maximum $|\alpha_0|^2$

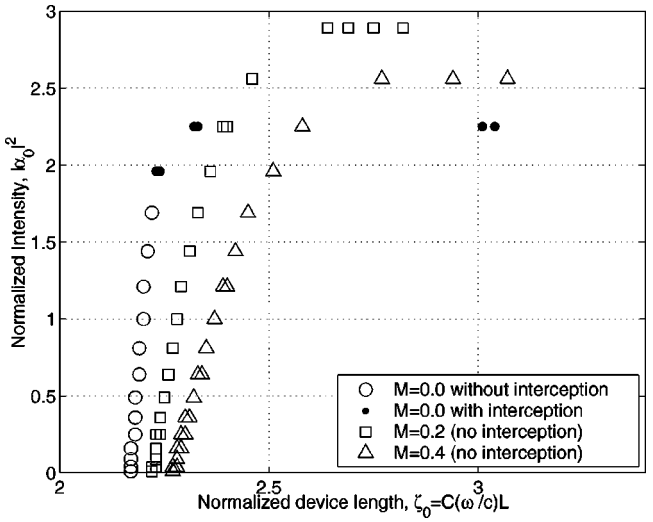

FIG. 5. Normalized intensity $|\alpha_0|^2$ versus the normalized BWO length ζ_0 for different values of the magnetic field parameter M. The BWO parameters used are initial normalized beam radius $\rho_0 = 2.0$, and normalized interception radius $\rho_{SWS} = 4.0$.

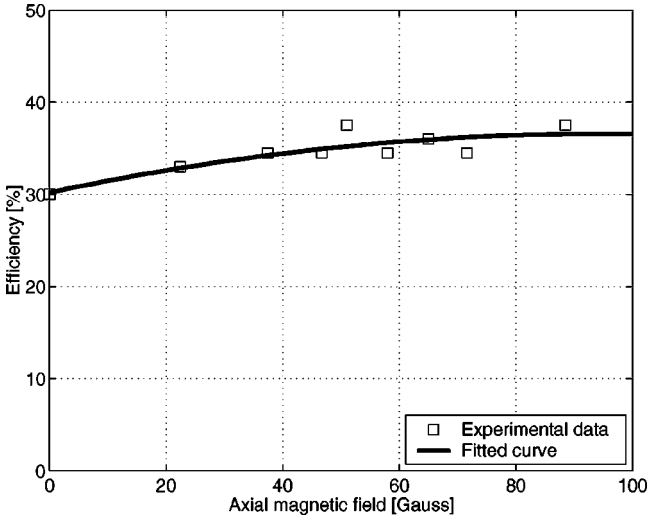

FIG. 6. Experimental results showing the increase of the PASOTRON efficiency with added weak axial magnetic field. The SWS is a helix with helix radius $r_H=2.5$ cm, pitch period $\lambda_H=2.2$ cm, and thickness $w_t=0.6$ cm. The assumed beam parameters are beam current $I_b=50$ A, beam voltage $V_b=40$ kV.

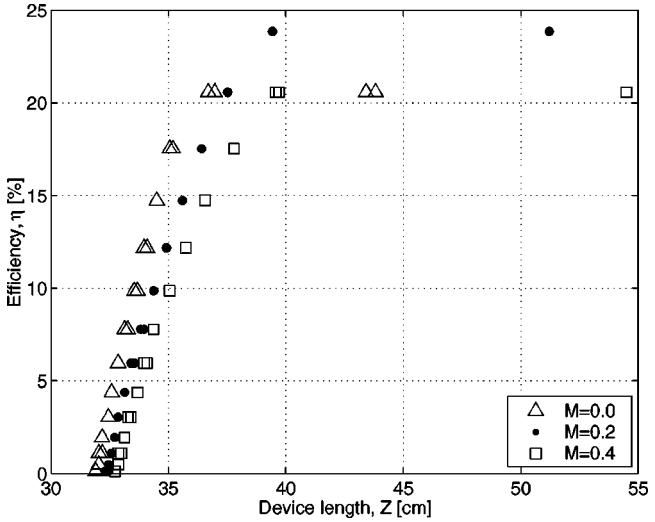

FIG. 7. The PASOTRON-BWO efficiency η versus its length Z for various values of the magnetic field parameter M. The SWS is a helix with helix radius $r_H=2.5$ cm, pitch period $\lambda_H=2.2$ cm, and thickness $w_t=0.6$ cm. The assumed beam parameters are beam current $I_b=50$ A, beam voltage $V_b=40$ kV, and initial radius $r_0=1.0$ cm. The device operates at 1.2 GHz.

achievable in this case is about 2.2. If we increase M to 0.2 the maximum $|\alpha_0|^2$ can reach up to 2.8, but this value is achievable for longer length of the device. Further increase of M does not help in enhancing the efficiency of the device. As shown in Fig. 5, at $M=0.4$ the maximum $|\alpha_0|^2$ is smaller than at $M=0.2$. This can be explained by the decrease in coupling between the electrons and the em wave with increase in M. No interception occurs for values of $M \geqslant 0.2$.

So far we have considered the BWO with zero reflection at the output end. In real devices, there are some reflections which, as shown in [8], typically reduce the starting current and slightly increase the efficiency. The first effect can be explained by the fact that reflections help to accumulate electromagnetic energy in the interaction space. The second effect becomes clear if we recall that the axial structure of the wave envelope with zero amplitude at the collector end is unfavorable for efficiency, since electron bunches, being modulated by the strong em field at the entrance, give up their energy to a weak em field at the exit.

V. EFFECT OF WEAK MAGNETIC FIELD ON THE EFFICIENCY OF A PASOTRON

Some of the theoretical results described in Sec. IV were compared with experimental observations in a helix PASOTRON [1,2] fitted with a weak ($B_z<100$ G) guiding magnetic field. The helix PASOTRON has the following parameters: helix radius=2.5 cm, pitch period=2.28 cm. The device was driven by a 50 A, 40 kV electron beam generated by a plasma electron gun. Under normal operating conditions ($B_z=0$) the output frequency is $f=1.29$ GHz, the output power is 600 kW, and the pulse duration is 80 μs. The guiding magnetic field is considered weak as long as $2\Omega/f \ll 1$ (the cyclotron frequency equals the radiation frequency at a magnetic field of $B_z=680$ G). Figure 6 shows the measured microwave power and efficiency as a function of the axial magnetic field. The microwave interaction efficiency increases monotonically from 30% ($B_z=0$) to 37% ($B_z=90$ G). For $B_z>90$ G, coherency of the output radiation is not maintained.

Thus the experimentally measured dependence of the microwave power on the magnetic field agrees reasonably well with the theoretical predictions. At the same time, it was found in the experiments that oscillations appear at distances shorter than the interaction distance, as can be seen in Fig. 7 (which shows the oscillations beginning to appear around 33 cm). In the experiments also the efficiency was higher than predicted by the theory. Both of these effects can be explained by wave reflections from the helix ends, as we discussed above. The theory also agrees with the experimentally measured Q factor of the existing helix with reflections. The value of this Q was found to be close to 400. If we assume that the diffraction Q factor can be estimated by the simple formula

$$Q \simeq \frac{\omega L}{v_{gr}(1-R)},$$

where R is the total reflection coefficient and the group velocity was experimentally measured to be $v_{gr} \simeq 0.143c$, then the known values of the operating frequency (1.266 GHz) and the helix length ($L=40$ cm) yield for the reflection coefficient $R \simeq 0.815$. In accordance with [7] and [8], such reflections should shorten the starting length by the factor $(1-R)^{1/3} \simeq 0.57$, i.e., almost twice. Such a correction of the distance shown in Fig. 7 makes these theoretical results well consistent with experimental observations.

We applied the BWO simulation described in Sec. IV B to a helix PASOTRON fitted with a weak guiding magnetic field. The coupling impedance of the annular electron beam with radius $r_0=1$ cm to the em wave was calculated by

using the code CHRISTINE [9], which gives $Z_c \approx 2.297\ \Omega$. This corresponds to a Pierce-like gain $C \approx 0.291$. Figure 7 shows the device efficiency versus its length for various values of the magnetic field parameter M. For the specific helix length of 40 cm, one can see an increase in the efficiency from 20% ($B_z = 0$) to about 24% ($B_z = 45$ G corresponds to $M = 0.2$).

VI. CONCLUSION

The operation of plasma-assisted TWT's and BWO's without a strong guiding axial magnetic field has the feature that the electrons can move radially toward the SWS under the influence of the rf fields. Furthermore, the transverse motion is dominated by transverse forces due to the rf fields. The proximity of electrons to the SWS increases the coupling between the electrons and the localized field near the SWS. Hence, the output power and the device efficiency increase, and the optimum interaction length shortens. However, this radial motion may lead to electron interception by the SWS, which is a major cause of output power saturation. We showed that adding a weak external magnetic field helps in optimizing operation in the regimes where we can increase the energy extraction from the beam before electron interception by the SWS occurs. We also showed that magnetic field tapering can reduce the optimum interaction length, which allows one to shorten the device.

For the BWO case, we showed that the additional external magnetic field is not always beneficial in enhancing the device efficiency, since the starting (and optimum) length increases with increasing magnetic field. Therefore, when the interaction length exceeds the starting length only slightly (for $M = 0$), the additional external magnetic field lowers the output power (it can even shut down the device operation). However, for relatively long devices, adding this weak external magnetic field (< 100 G) can enhance the device output power and efficiency. The latter was also demonstrated experimentally.

ACKNOWLEDGMENTS

This work was supported by the Air Force Office for Scientific Research. The authors wish to thank J. Rodgers for his help in experimental studies and V. L. Granatstein for his valuable comments.

[1] D. M. Goebel *et al.*, IEEE Trans. Plasma Sci. **22**, 547 (1994).
[2] D. M. Goebel *et al.*, IEEE Trans. Plasma Sci. **27**, 800 (1999).
[3] W. H. Bennett, Phys. Rev. **45**, 890 (1934).
[4] J. R. Pierce, in *Traveling-Wave Tubes* (Van Nostrand, Toronto, 1950), Chap. 13, p. 173.
[5] G. S. Nusinovich and Y. P. Bliokh, Phys. Rev. E **62**, 2657 (2000).
[6] N. F. Kovalev and A. V. Smorgonskiy, Radio Eng. Electron. Phys. **20**, 133 (1974).
[7] H. R. Johnson, Proc. IRE **684** (1955).
[8] B. Levush *et al.*, IEEE Trans. Plasma Sci. **20**, 263 (1992).
[9] D. Chernin, T. M. Antonsen, Jr., and B. Levush, IEEE Trans. Electron Devices **46**, 1472 (1999).